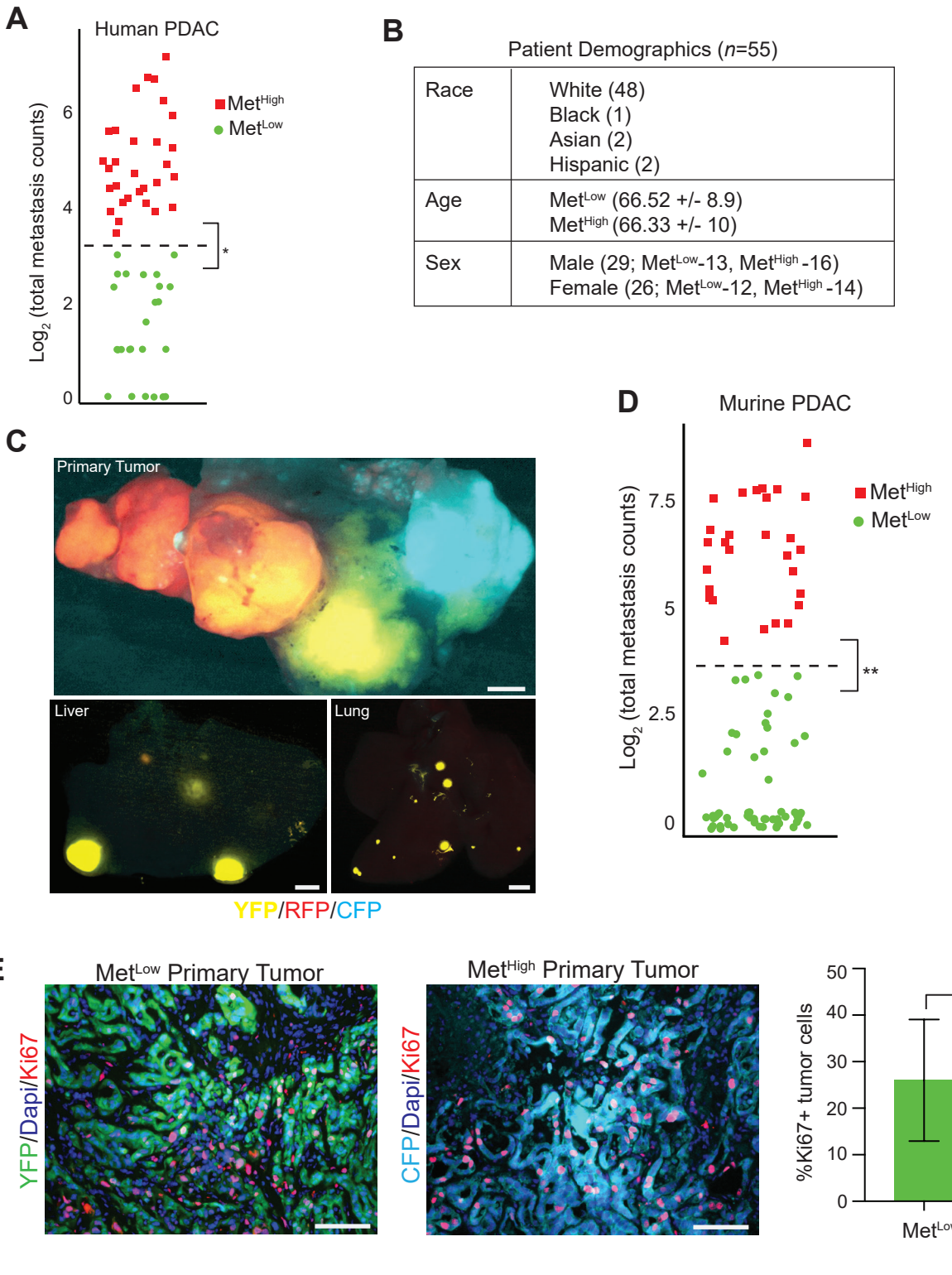

Supplementary Figure S1: Classifying metastatic burden in human and murine advanced PDAC. (A) K-means clustering of human PDAC metastasis counts demonstrating two distinct clusters with Met^{Low} ≤10 and Met^{High} >10 total (liver and lung) metastasis (n=55 patients). **(B)** Demographics (age of diagnosis, sex, and race) of the patients analyzed in Fig. 1A-D and Fig. S1A. **(C)** Representative stereomicroscopic fluorescent image showing multiple primary tumors (RFP^+, YFP^+, and CFP^+) in the pancreas with matched metastases in the liver and lung. Liver and lung metastases are derived primarily from the YFP+ tumor. **(D)** K-means clustering of murine PDAC metastasis counts demonstrating two distinct clusters that are defined as having high or low metastatic burden. Met^{Low} ≤10 and Met^{High} >10 total (liver and lung) metastasis (n=85 tumor clones). **(E)** Ki67 staining in primary Met^{Low} and Met^{High} tumors with representative IF images (left) and counts (right). Data from n=3 Met^{Low} and n=3 Met^{High} primary tumors and 4-5 random fields of view. Statistical analysis by Student's unpaired t-test with significance indicated (ns, not significant). Error bars indicate SEM. Scale bars: 1mm for S1C and 50μm for S1E.

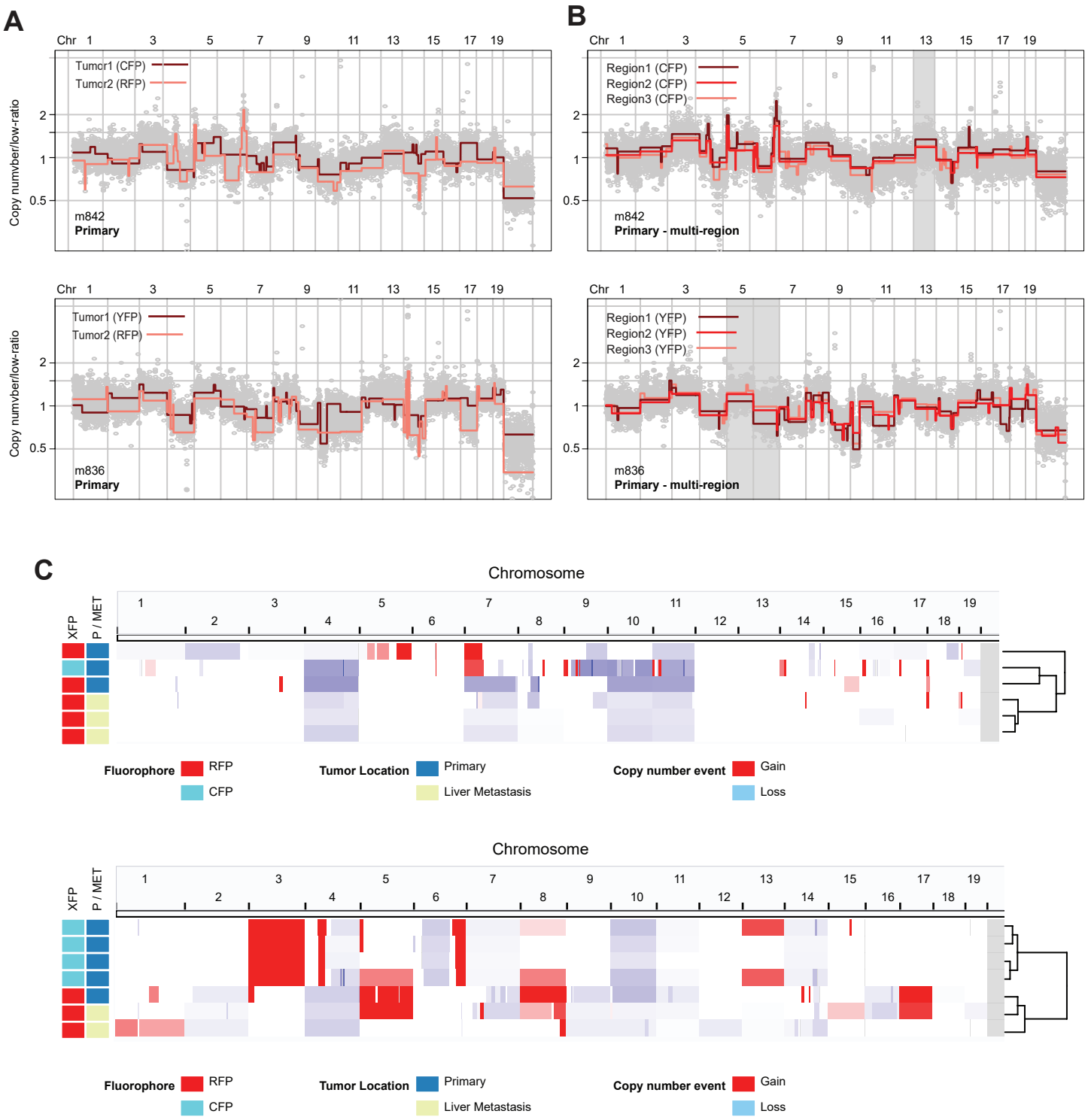

Supplementary Figure S2. Copy number alteration analysis reveals lineage relationships and genetic heterogeneity of fluorescently labeled primary PDACs and their matching metastases. (A) Overlay of genome-wide copy number profiles of different fluorescently labeled (CFP and RFP) primary tumors from mouse 842 (m842 - top panel) and mouse 836 (m836 - bottom panel) illustrating differing rearrangement profiles. **(B)** Overlay of genome-wide copy number profiles of tumors where multi-region sampling was performed. Top panel illustrates three CFP sub-samples from CFP tumor mass from m842. Bottom panel illustrates three YFP sub-samples from a YFP tumor mass from m836. **(C)** Genome-wide heatmap with hierarchal clustering based on copy number alterations of matched primary and metastatic samples profiled from m471 (top panel) and m842 (bottom panel). Color codes for Flourescence label, primary/metastatic designation, and nature of copy number alteration are provided below.

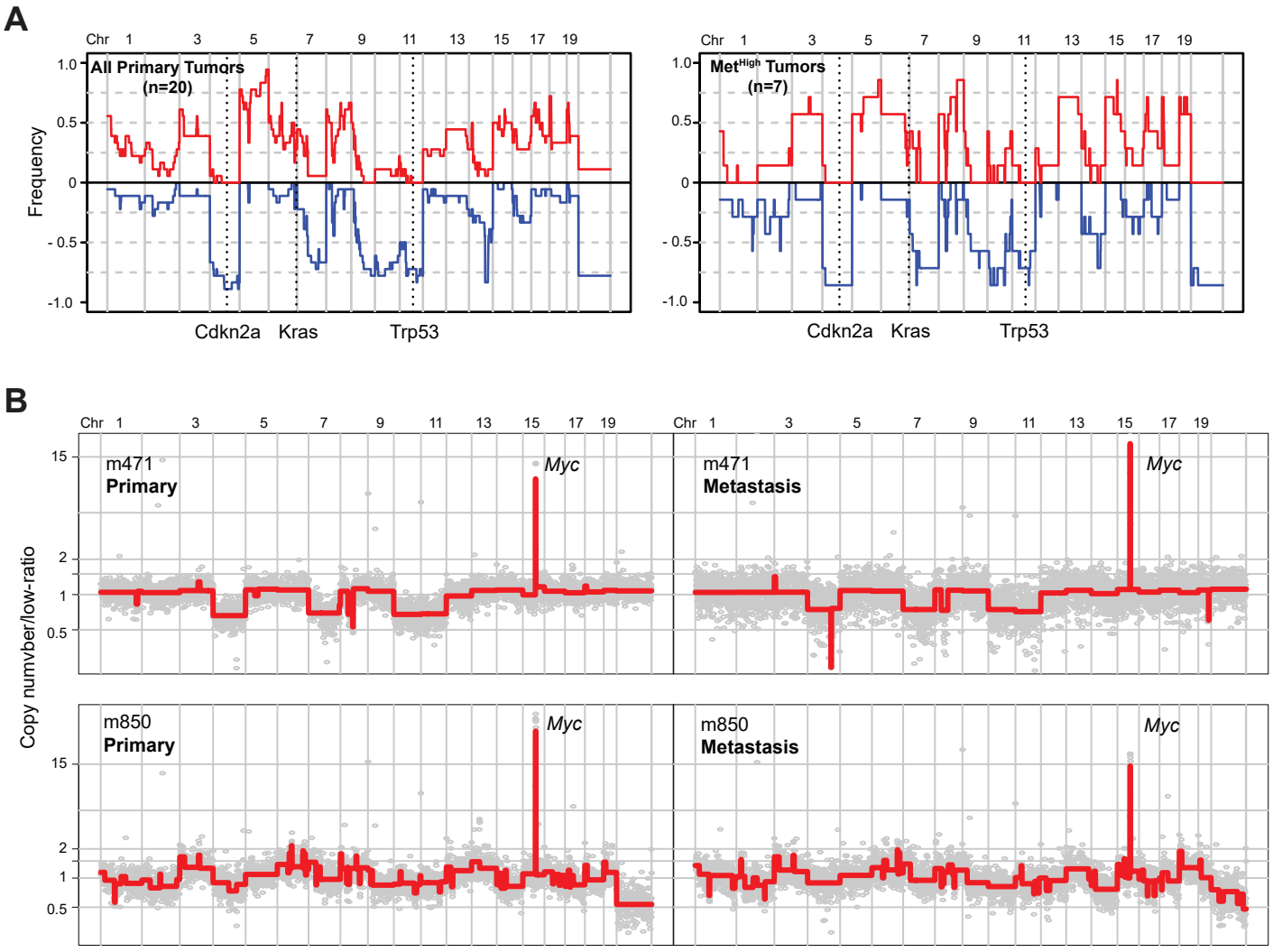

Supplementary Figure S3: Global patterns of large scale copy number alterations do not differ between Met^{High} and Met^{Low} clones, while *Myc* amplifications are maintained in metastatic lesions. (A) Genome-wide frequency plot illustration of large scale copy number events found in all primary tumors (left panel) and in Met^{High} (right panel) primary tumors. Alterations in *Cdkn2a*, *Kras*, and *Trp53* are noted on the plots. **(B)** Genome-wide copy number profiles of matching Met^{High} primary tumors (left panels) and paired liver metastases (right panels) from different examined mice. *Myc* amplifications are noted on profiles.

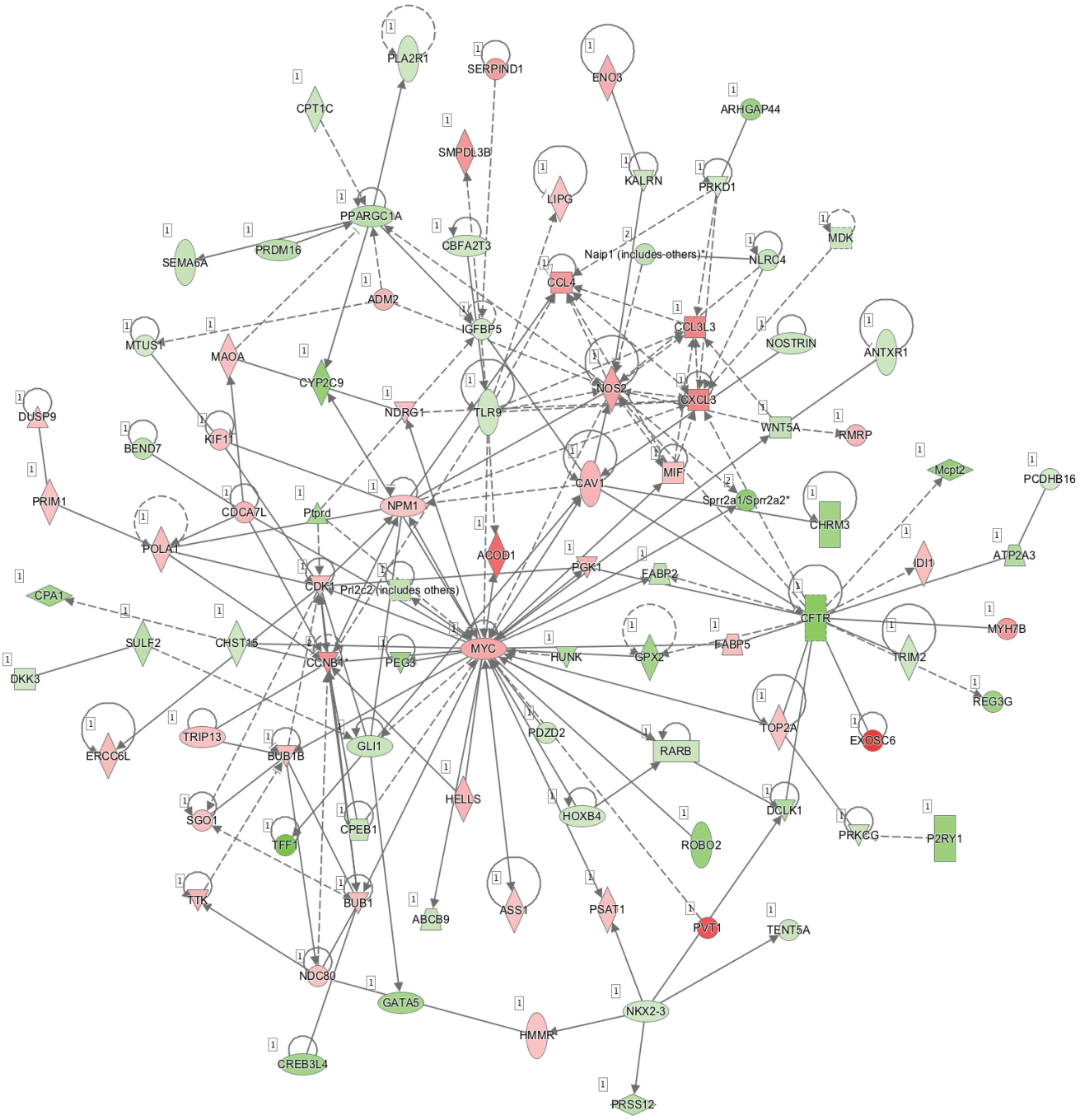

Supplementary Figure S4: Ingenuity pathway analysis of the Met^{High} transcriptome.

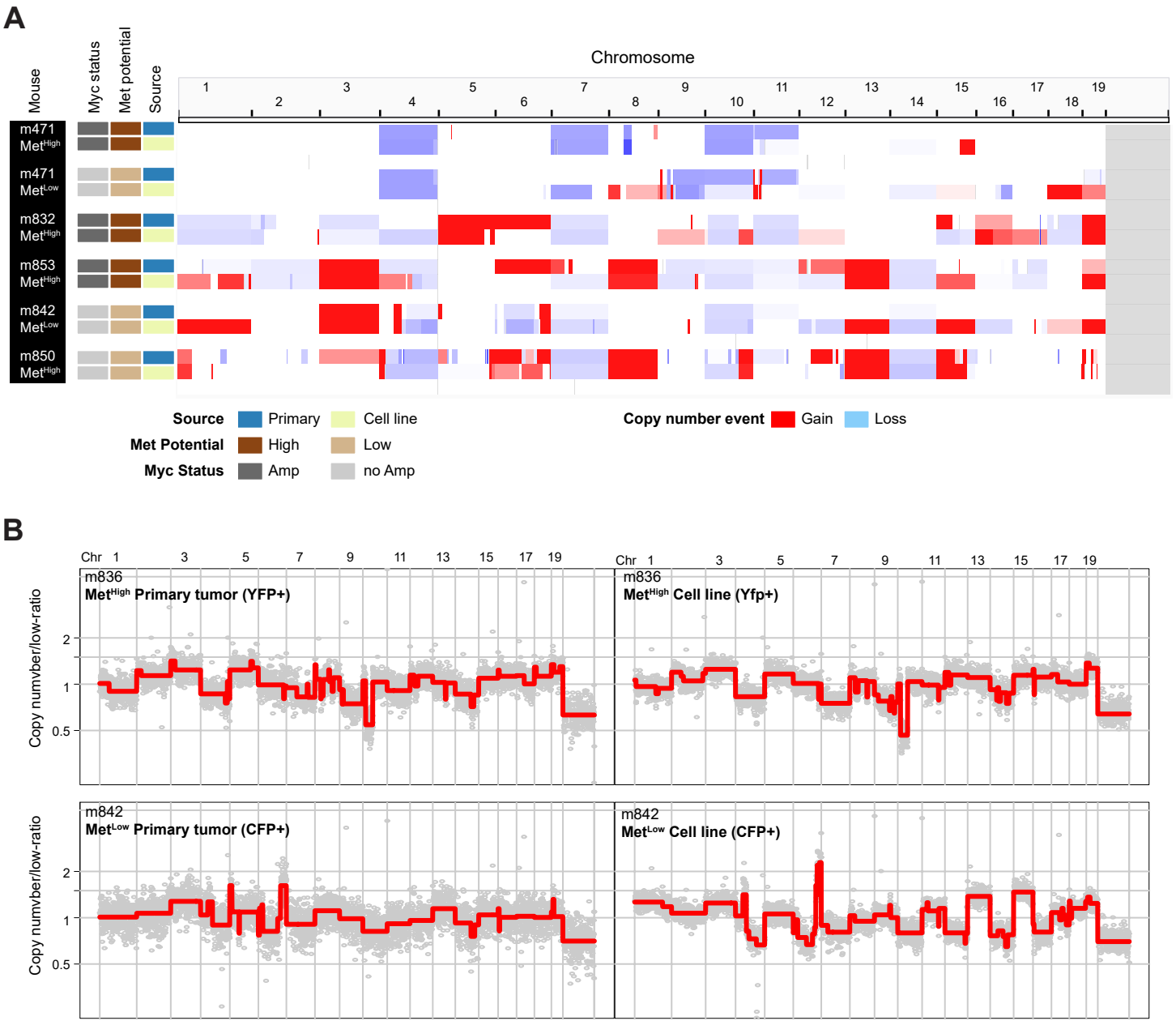

Supplementary Figure S5: Established Met^{High} / Met^{Low} cell lines maintain their overall genomic profile and do not select for *Myc* amplification during in vitro culture. (A) Schematic representation of genome wide copy number profile of matching primary tumor and cell lines samples illustrating the maintenance of their overall copy number pattern. **(B)** Representative genome-wide copy number profiles of matching primary tumors and cell line samples for a Met^{High} tumor from m836 (YFP+) and Met^{Low} tumor from m842 (CFP+), top and bottom panels, respectively.

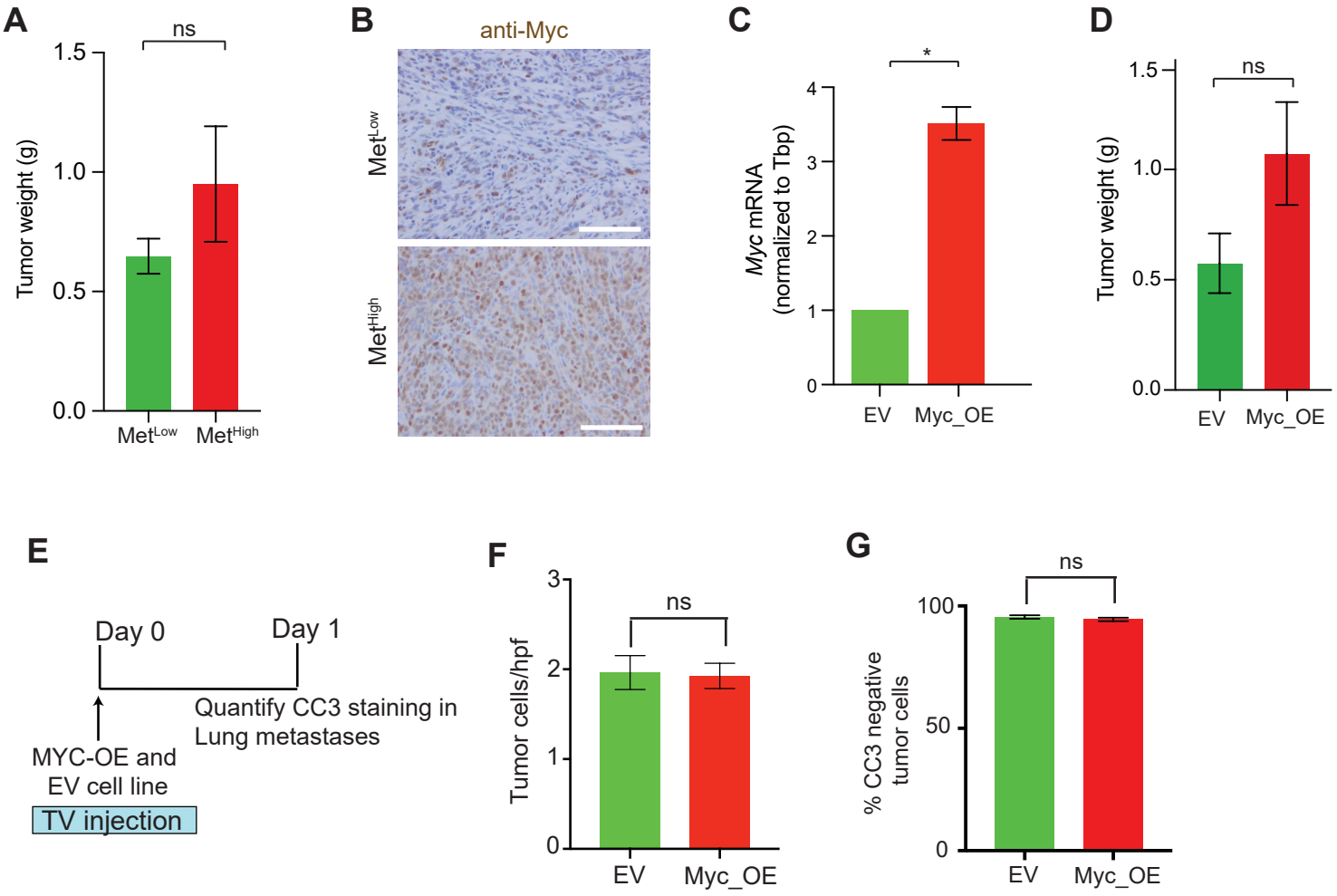

Supplementary Figure S6: Tumor weight, *Myc* expression, and CTC survival in orthotopic primary tumors primary and Myc overexpressing cell lines **(A)** Tumor weight in grams of Met^{Low} and Met^{High} cell line-derived orthotopic tumors in Figure 4C (n= 4 Met^{Low} and 5 Met^{High} cell lines). **(B)** Representative Myc IHC staining of Met^{Low} and Met^{High} orthotopic tumors. **(C)** *Myc* gene expression in Met^{Low}-derived Myc_OE and EV cell lines (n=4 each). **(D)** Weights of Myc_OE and EV cell line-derived orthotopic tumors from Figure 4D. **(E)** Schematic outline of an experiment to assess survival of circulating tumor cells. 471 Myc_OE and EV lines were injected by tail vein (n= 2 EV and n=2 Myc_OE lines) into NOD.SCID mice and the lungs were assessed 24 hours later, **(F-G)** Quantification of YFP+ cells **(F)** and cleaved caspase-3- cells (**G**) from the experiment in **(E)** (15 random fields of view analyzed). Statistical analysis by Student's unpaired t-test with significance indicated (*, p=0.007; ns, not significant). Error bars indicte SEM. Scale bar: 50μm (**B**).

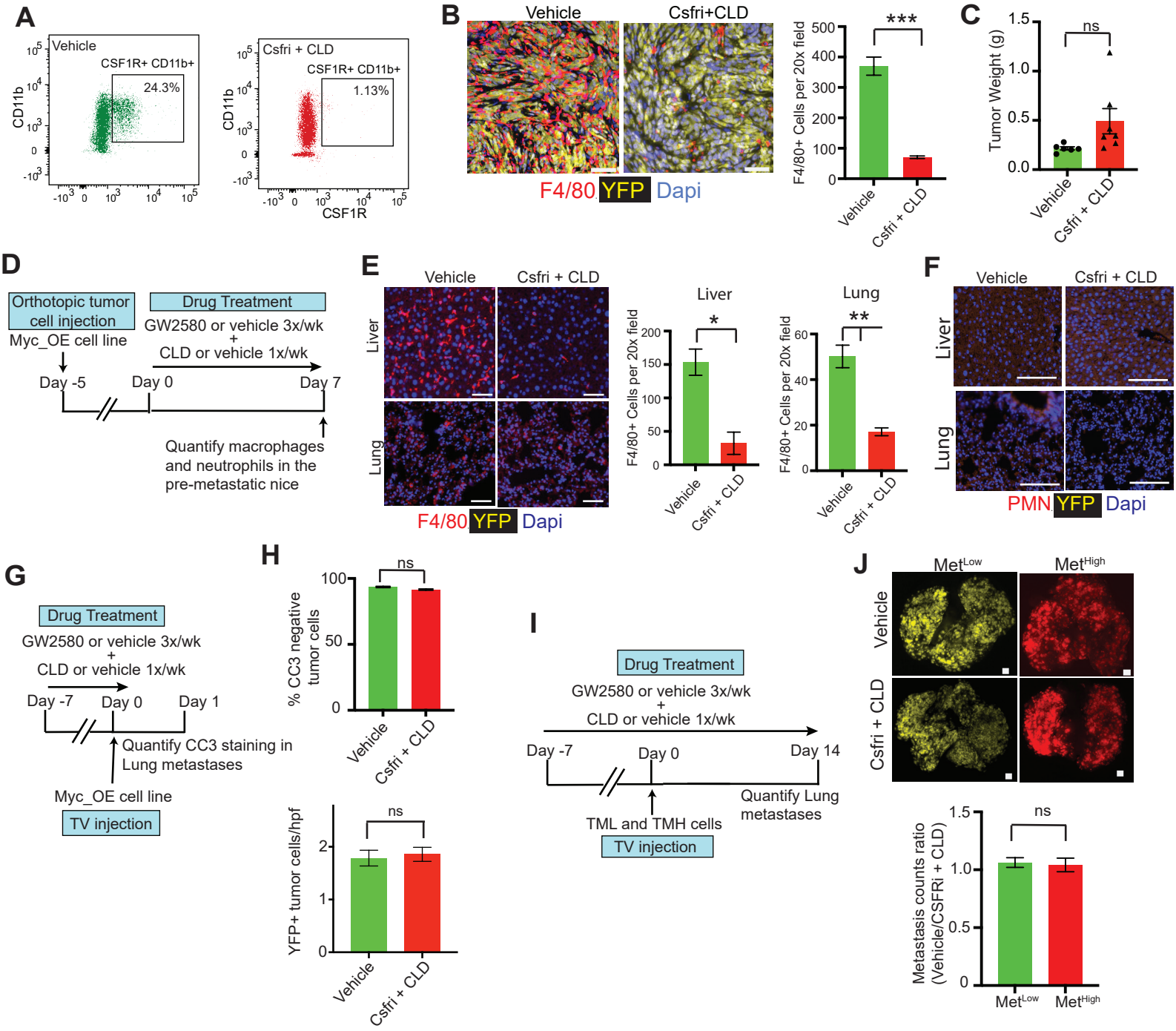

Supplementary Figure S7: TAM depletion does not affect CTC survival or metastatic colonization: (A) Representative flow cytometry dot plots showing relative abundance of CSFR1+CD11b+ macrophages in the circulation following treatment with GW2580+CLD or vehicle as described in Fig. 5J. **(B)** Representative immunofluorescence images (left) and quantification (right) demonstrating depletion of TAMs (F4/80+) cells from liver following the macrophage depletion strategy outlined in Fig. 5iJ (n=4 control mice and n=4 GW2580+CLD mice from 2 independent cell lines were examined; 4-5 random fields of view analyzed). **(C)** Weights of orthotopic tumors following treatment as described in Fig 5J (n=6 vehicle and n=7 GW2580+CLD treated tumors **(D)** Schematic outline of a macrophage depletion experiment to evaluate effect on TAMs on the premetastatic niche. Mice were orthotopically implanted with Myc_OE cells (n=2 independent cell lines) and after 5d were treated with a combination of GW2580 + CLD or vehicle. F4/80+ TAMs in liver and lung pre-metastatic niche were examined 7 days later by immunofluorescence. **(E)** Representative images and quantification of F4/80+ TAMs (n=4 control mice and n=4 GW2580+CLD mice). **(F)** Representative images of anti-neutrophil antibody (neutrophils) staining in livers and lungs from orthotopic tumors described in (**D**). **(G)** Schematic outline of a macrophage depletion experiment to evaluate the effect of macrophage depletion on CTC survival. Mice were treated with a combination of GW2580+CLD or vehicle for 7d followed by tail vein injection of the 471 Myc_OE cell line. After 24h, cleaved caspase-3+ cells (**H**, top panel) and single YFP+ cells (**H**, bottom panel) were quantified (15 20x random fields of view were analyzed). **(I)** Schematic outline of an experiment to evaluate effect of macrophage depletion on metastatic colonization and growth. Mice were treated with a combination of GW2580+CLD or vehicle for 7d followed by tail vein injection of Met^{High} and Met^{Low} cells (n=2 independent $MMet^{High}$ and Met^{Low} cell lines). Treatment continued for an additional 14d at which time lung metastases were quantified. **(J)** Representative fluorescent stereomicroscope images and quantification of the experiment in (**I**) (n=6 control mice and n=7 GW2580+CLD mice). Statistical analysis by Student's unpaired t-test with significance indicated (*, p=0.0065; **; p=0.0042; ***; p<0.0001; ns, not significant). Error bars indicate SEM. Scale bars: 50μm (panels **B, D, E**) and 1mm (panel **J**).

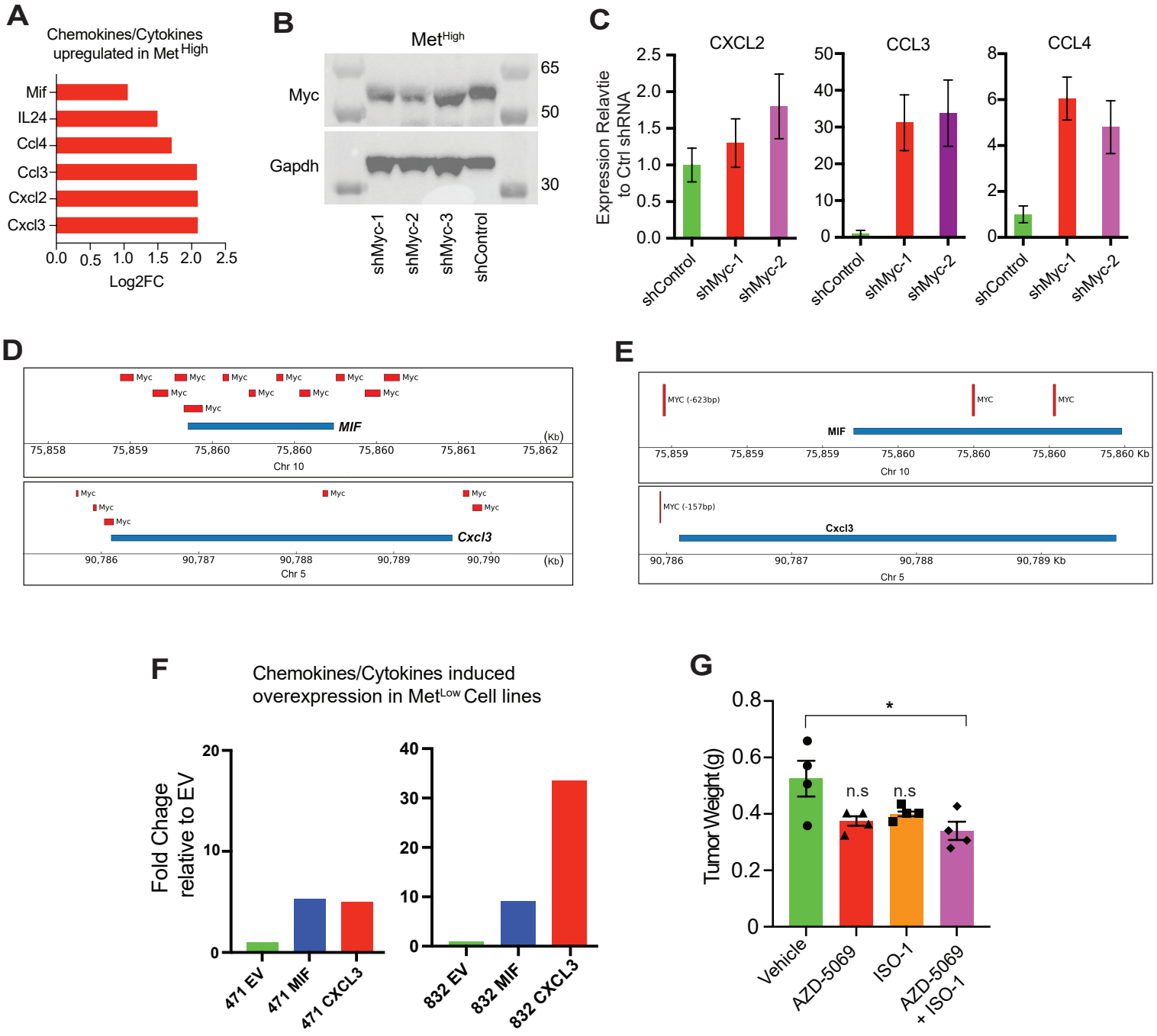

Supplementary Figure S8: Chemokines/cytokines regulated by Myc in Met^{High} tumors: (A) Chemokines/cytokines exhibiting elevated expression (logfold-change >1, Padj <0.01) Met^{High} tumors compared to Met^{Low} tumors (as described in Fig. 3). **(B)** Representative western blot of Myc protein levels in a Met^{High} cell line stably transduced with one of three shRNAs directed against *Myc* (shRNA1, 2, 3) or a scrambled shRNA (shControl). shRNA 1 and 2 provided the most significant decrease in Myc protein levels and were used in the experiments in Fig. 6B. **(C)** Relative expression of Cxcl2, Ccl3, and Ccl4 in *Myc* shRNA Met^{High} cell lines compared to scrambled shRNA control from. Data are representative of 2 independent *Myc* shRNAs in a Met^{High} cell line. **(D-E)** MYC binding sites (red boxes) in the promoter regions of MIF and CXCL3 identified in the Gene Transcription Regulation Database (GTRD) from ChIPseq analysis (**D**) and Motif finding analysis of Eukaryotic Promoter Database (EPD) (**E**). **(F)** Relative Mif and Cxcl3 expression in Cxcl3_OE, Mif_OE, and EV cells in Fig. 6D-E. **(G)** Tumor weights of 832 Myc_OE tumor cell-derived orthotopic tumors treated with either Vehicle, AZD-5069, ISO-1, or AZD-5069+ISO-1 (Fig. 6G-J). Statistical analysis by Student's unpaired t-test with significance indicated (*, p=0.04; ns, not significant). Error bars indicate SEM.

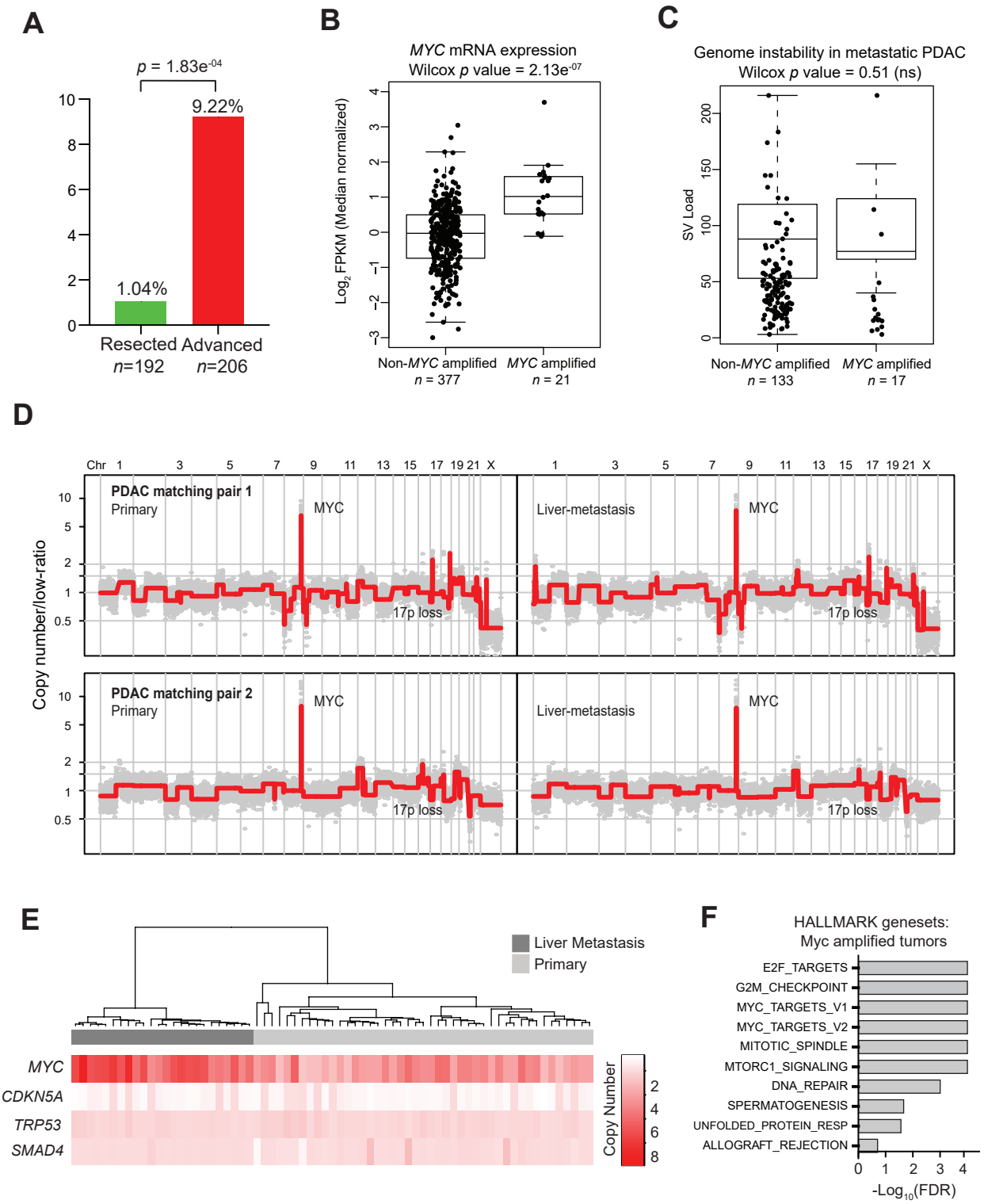

Supplementary Figure S9: ***MYC*** **amplifications are enriched in metastatic human PDA. (A)** Bar graph showing the relative frequencies of MYC amplifications in resected and advanced PDAC tumors from the COMPASS cohort. **(B)** *MYC* expression in non-MYC amplified and MYC amplified tumors in the COMPASS cohort. **(C)** Measurement of total structural variant burden in non-MYC amplified and MYC amplified tumors in the COMPASS cohort. **(D)** Genome-wide relative copy number profiles of two patients with matched primary PDAC (left) and liver metastasis (right). **(E)** Heatmap depiction of *MYC*, *CDKN5A*, *TRP53*, and *SMAD4* copy number alteration in cancer single cells sequenced from a matched primary PDAC and its liver metastasis depicted in Fig. 7E. Color codes indicate absolute copy number in single-cells. Top bar plot depicts tissue site from which single-cells were retrieved. **(F)** Gene set enrichment analysis of MYC amplified tumors (compared to non-amplified tumors) in the COMPASS cohort.